Transmembrane Domain of M2 Protein from Influenza A Virus Studied by Solid-State ^{15}N Polarization Inversion Spin Exchange at Magic Angle NMR

Zhiyan Song,* F. A. Kovacs,† J. Wang,† Jeffrey K. Denny,*‡ S. C. Shekar,§ J. R. Quine,*†‡ and T. A. Cross*†¶
*National High Magnetic Field Laboratory, †Institute of Molecular Biophysics, ¶Department of Chemistry, and ‡Department of Mathematics, Florida State University, Tallahassee, Florida 32306; and §Department of Biochemistry and Cellular Biology, State University of New York, Stony Brook, New York 11794 USA

ABSTRACT The M2 protein from the influenza A virus forms a proton channel in the virion that is essential for infection. This tetrameric protein appears to form a four-helix bundle spanning the viral membrane. Here the solid-state NMR method, 2D polarization inversion spin exchange at magic angle (PISEMA), has been used to obtain multiple constraints from specifically amino acid-labeled samples. The improvement of spectral resolution from 2D PISEMA over 1D methods and 2D separated local field methods is substantial. The reliability of the method is validated by comparison of anisotropic chemical shift and heteronuclear dipolar interactions from single site labeled samples. The quantitative interpretation of the high-resolution constraints confirms the helix tilt to be within the range of previous experimental determinations (32°–38°). The binding of the channel inhibitor, amantadine, results in no change in the backbone structure at position $Val_{27,28}$, which is thought to be a potential binding site for the inhibitor.

INTRODUCTION

The efficient utilization of structural constraints and incorporation of all structural information into structural modeling is an ongoing challenge. The solid-state NMR method, polarization inversion spin exchange at magic angle (PISEMA), which correlates ^{15}N-^{1}H dipolar interactions with ^{15}N chemical shifts (Wu et al., 1994), provides high-resolution orientational constraints. Here these constraints are obtained for the transmembrane peptide of M2 protein from influenza A virus, M2-TMP. Through assignments made by single-site labels, these high-resolution constraints are combined with the known α-helical structure of M2-TMP to enhance a structural model and to determine specific torsion angles.

While distance and torsional constraints can be obtained by solid-state NMR from unoriented samples, orientational constraints in this paper are obtained from samples uniformly aligned with respect to the magnetic field axis of the NMR spectrometer. Such constraints have numerous advantages for assembling structures and for obtaining a structure that is oriented with respect to its environment—in this molecular system, a lipid bilayer (Fu and Cross, 1999; Quine, 1999).

The two-dimensional PISEMA pulse sequence, developed by Opella and co-workers, has been successfully used to obtain anisotropic ^{15}N chemical shifts and directly bonded ^{15}N-^{1}H dipolar interactions (Wu et al., 1994; Marrassi et al., 1997; Tian et al., 1998). This spectroscopy of uniformly aligned samples yields much improved dipolar resolution and a favorable dipolar scaling factor (0.816) compared to earlier separated local field (SLF) spectroscopy (Hester et al., 1976; Waugh, 1976). The scheme uses conventional I-S cross-polarization (CP) followed by frequency-switched Lee-Goldburg (LG) cycles (Bielecki et al., 1990; Lee and Goldburg, 1965). During the LG cycles, the I-spins are locked along the magic angle, 54.74° relative to the magnetic field, and matched by a phase-alternated spin-lock field applied to the S-spins. The Fourier transform of the NMR signal against acquisition time, t_2, and evolution time, t_1, yields a 2D spectrum with chemical shifts in the ω_2 dimension and dipolar splittings in the ω_1 dimension.

The M2 protein (97 amino acids) from the influenza A virus is an integral membrane protein with proton channel activity in the viral coat (Lamb et al., 1994; Wang et al., 1994). Its single transmembrane α-helix is contained within the 25-amino acid peptide M2-TMP (residues 22–46), which has been reported to show channel activity similar to that of native M2 protein (Duff and Ashley, 1992). However, recent studies of various truncated proteins have brought this result into question (Tobler et al., 1999). The transmembrane portion of both M2 and M2-TMP primarily adopts an α-helical structure, and M2 forms a homotetramer in lipid environments, as characterized by several studies (Duff et al., 1992; Holsinger and Lamb, 1991; Sakguchi et al., 1997; Kovacs and Cross, 1997). M2-TMP also appears to form an oligomer. The helix tilt of a monomer should be sensitive to the thickness of the lipid bilayer, but M2-TMP has been shown to be quite insensitive to a change in bilayer thickness (Kovacs et al., 2000). Therefore, the helix tilt appears to be an intrinsic propensity of an oligomer. In addition, the oligomer is not a heterogeneous aggregate, inasmuch as single site labels give rise to a single identical

Received for publication 20 December 1999 and in final form 11 April 2000.

Address reprint requests to Dr. Timothy A. Cross, National High Magnetic Field Laboratory, Florida State University, 1800 E. Paul Dirac Drive, Tallahassee, FL 32306-4005. Tel.: 850-644-0917; Fax: 850-644-1366; E-mail: cross@magnet.fsu.edu.

0006-3495/00/08/767/09 $2.00

resonance from each monomer. M2-TMP is therefore presumed to be a tetrameric state, similar to M2 protein, but the oligomeric state of M2-TMP has not been specifically defined.

In previous investigations of isotopically labeled M2-TMP, orientational constraints derived from NMR and infrared spectroscopy were interpreted to show that the helices are tilted by 32°–38° with respect to the lipid bilayer normal (Kovacs and Cross, 1997; Kukol et al., 1999; Kovacs et al., 2000). Moreover, model building of the tetramer suggested that the α-helical bundle is left-handed (Kovacs and Cross, 1997). The channel function of M2 can be blocked by amantadine, potentially through binding to a specific sequence (residues 27–31) in its transmembrane domain (Skehel, 1992; Hay, 1992; Wang et al., 1993). Here a preliminary binding experiment of amantadine with M2-TMP is described.

MATERIALS AND METHODS

Sample preparation

Several ^{15}N-labeled amino acids were purchased from Cambridge Isotope Lab (Cambridge, MA). M2-TMP (NH_2-Ser^{22}-Ser^{23}-Asp^{24}-Pro^{25}-Leu^{26}-Val^{27}-Val^{28}-Ala^{29}-Ala^{30}-Ser^{31}-Ile^{32}-Ile^{33}-Gly^{34}-Ile^{35}-Leu^{36}-His^{37}-Leu^{38}-Ile^{39}-Leu^{40}-Trp^{41}-Ile^{42}-Leu^{43}-Asp^{44}-Arg^{45}-Leu^{46}-CO_2H) was obtained by solid-phase synthesis, using fluorenoylmethoxy carbonyl chemistry on an Applied Biosystems 430A Synthesizer. Amino acid blocking, purification, and characterization of the peptides were performed as previously described (Kovacs et al., 2000).

To orient a lipid bilayer preparation, M2-TMP and dimyristoylphosphatidylcholine (DMPC) or dioleoylphosphatidylcholine (DOPC) were codissolved in trifluoroethanol (TFE) with a peptide-to-lipid molar ratio of 1:8 and 1:30, respectively. Then the sample was spread onto ~60 thin glass plates (75 μm × 10.5 mm × 10.5 mm). After vacuum drying to remove TFE, the glass plates were stacked into a glass tube (11 mm × 11 mm), and the samples were hydrated with high-performance liquid chromatography-grade water (~50% by weight). Finally, the samples were sealed and incubated at ~45°C for several days.

NMR experiments

The NMR measurements were performed on a spectrometer with a 9.4-T magnet, operating at a ^{15}N Larmor frequency of 40.585 MHz. The probe was constructed in house and has a rectangular coil suited to the sample size. The oriented M2-TMP samples were placed with the order axis (i.e., the lipid bilayer normal) parallel to the magnetic field axis. All ^{15}N chemical shifts are relative to the resonance for a saturated solution of $^{15}NH_4NO_3$ at 0 ppm.

For the PISEMA experiment, the cross-polarization (CP) period was 1 ms. The rf field strengths were typically 31.4 kHz for the CP match and 38.5 kHz for the Lee-Goldburg (LG) condition, corresponding to a LG time interval of $t_m = 26$ μs. A delay of 1 μs was used at the onset of each $\pm$LG cycle to compensate for the frequency synthesizer (Programmed Test Sources type) switch time, which was found to be critical for achieving the theoretical dipolar scaling factor (0.816). The t_1 value was incremented from 0 to 24 Lee-Goldburg cycles, and the refocused ^{15}N-signal was acquired with ~2000 transients for each t_1 increment. For data processing, 512 and 256 points in the t_2 and t_1 dimensions were used, respectively, and exponential line broadening of 100 Hz was used in the t_2 dimension, but not in the t_1 dimension. The spectral symmetry in the dipolar dimension was achieved by setting the imaginary portion of the data points to zero before the Fourier transform against t_1.

ANALYSIS OF 2D SPECTRA

For spectral analysis, several relevant orientation reference frames are defined (Fig. 1) as follows: **P**, the ^{15}N chemical shift anisotropy (CSA) principal axis frame with the principal tensor elements σ_{11}, σ_{22}, σ_{33}; **Nh**, the frame of the ^{15}N-^{1}H dipolar interaction tensor with its unique z axis along the ^{15}N-^{1}H bond; **D**, the director frame with its z axis along the lipid bilayer normal. Any two of these coordinate systems are related by Euler rotations $\Omega(\alpha, \beta, \gamma)$.

In our oriented samples, the z axis of the director frame is parallel to the magnetic field, $\mathbf{B}_0$, and the observed chemical shift can be written in terms of tensor magnitudes and orientations as

$$\sigma_{obs} = \sigma_{11}\cos^2\alpha_{PD}\sin^2\beta_{PD} + \sigma_{22}\sin^2\alpha_{PD}\sin^2\beta_{PD} + \sigma_{33}\cos^2\beta_{PD} \quad (1)$$

where the Euler angles α_{PD}, β_{PD} relate the CSA principal axis frame to the sample director frame. Notice that $\gamma_{PD} = 0$.

The ^{15}N-^{1}H dipolar splitting can be described by

$$\Delta\nu = \pm \nu_{\parallel}(3\cos^2\theta - 1) \quad (2)$$

where $\nu_{\parallel} = (\mu_0/4\pi)(\gamma_H\gamma_N h/2\pi r_{NH}^3)$ is the dipolar coupling constant; γ_H and γ_N are the gyromagnetic ratios of ^{1}H and ^{15}N, respectively; h is Planck's constant; and r_{NH} is the N-H bond length. The angle θ is the polar angle relating the N-H internuclear vector to $\mathbf{B}_0$. Correlating with the CSA frame

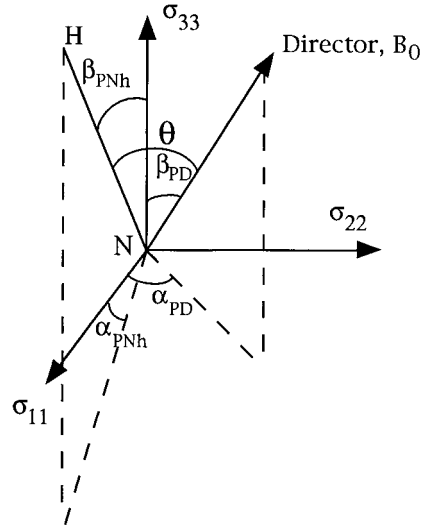

FIGURE 1 Definition of the ^{15}N chemical shift principal axis frame (PAS) and the ^{15}N-^{1}H dipolar interaction tensor with respect to the sample director axis. This latter axis is the bilayer normal in the samples studied here, and it is arranged to be parallel to $\mathbf{B}_0$.

yields

$$\cos\theta = \cos\beta_{PD}\cos\beta_{PNh} + \sin\alpha_{PD}\sin\beta_{PD}\sin\alpha_{PNh}\sin\beta_{PNh} + \cos\alpha_{PD}\sin\beta_{PD}\cos\alpha_{PNh}\sin\beta_{PNh} \quad (3)$$

where the Euler angles (α_{PD}, β_{PD}) and (α_{PNh}, β_{PNh}) refer to the transformation from the CSA principal axis frame to the director frame and to the dipolar tensor frame, respectively.

Taking the ^{15}N-^{1}H dipolar coupling constant to be $\nu_{\parallel}$ = 10.735 kHz, based on an N-H bond length of 1.041 Å, and assuming that the ^{15}N amide tensor orientations relative to the ^{15}N-^{1}H bond are typically $\alpha_{PNh} = 0°$, $\beta_{PNh} = 17°$ (Mai et al., 1993), Eqs. 1–3 can be solved for each site, using pairs of (σ_{obs}, $\Delta\nu$) values obtained from 2D PISEMA and the corresponding CSA tensor values σ_{11}, σ_{22}, σ_{33}. The resulting θ and (α_{PD}, β_{PD}) values relate the N-H bond and the CSA principal axis frame, respectively, to the director z axis. These angles give important orientational constraints for structural analysis. In general, four possible α_{PD}, β_{PD} solutions, ($\pm\alpha_{PD}$, β_{PD}), ($\pi \pm \alpha_{PD}$, $\pi - \beta_{PD}$), may be derived from the combination of Eqs. 1–3, while two solutions, (θ, $\pi - \theta$), may be derived from a positive dipolar splitting value according to Eq. 2. For two adjacent residues, such as Val$^{27–28}$ and Ile$^{32–33}$, the orientations of the principal axis frames for each residue can be used to obtain a list of possible ϕ, ψ torsion angles that correspond to the data for those residues.

The PAF_1 is defined as the CSA principal axis frame for the first residue (either Val^{27} or Ile^{32}) with the $\mathbf{B}_0$ orientation (α_{PD1}, β_{PD1}), and the PAF_2 is the CSA principal axis frame for the second residue (Val^{28} or Ile^{33}) with the $\mathbf{B}_0$ orientation (α_{PD2}, β_{PD2}). For the peptide plane geometry in Fig. 2, the supplements of the bond angles C_α-C_1-N and C_1-N-C_α are 65° and 59°, respectively, and the tetrahedral geometry at C_α is such that the supplement of the angle N-C_α-C is 70°. Unit vectors in the direction of the C_1-N and N-C_α bonds in PAF_1 are denoted by $\mathbf{u}_1$ and $\mathbf{u}_2$, and the unit vectors in the direction of the C_α-C_1 and C_1-N bonds in PAF_2 are denoted by $\mathbf{u}_3$ and $\mathbf{u}_4$.

Based on four possible α_{PD}, β_{PD} solutions for each pair of residues, the torsion angles can now be computed by using orientational constraints and a torsion angle identity:

$$\begin{aligned}\phi &= \mathrm{Tor}(\mathbf{u}_1,\mathbf{u}_2,\mathbf{u}_3) = \mathrm{Tor}(\mathbf{u}_1,\mathbf{u}_2,\mathbf{B}(\alpha_{PD1},\beta_{PD1})) \\ &\quad + \mathrm{Tor}(-\mathbf{B}(\alpha_{PD1},\beta_{PD1}),\mathbf{u}_2,\mathbf{u}_3) \\ \psi &= \mathrm{Tor}(\mathbf{u}_2,\mathbf{u}_3,\mathbf{u}_4) = \mathrm{Tor}(\mathbf{u}_2,\mathbf{u}_3,\mathbf{B}(\alpha_{PD2},\beta_{PD2})) \\ &\quad + \mathrm{Tor}(-\mathbf{B}(\alpha_{PD2},\beta_{PD2}),\mathbf{u}_3,\mathbf{u}_4) \end{aligned} \quad (4)$$

where

$$\mathrm{Tor}(\mathbf{v}_1,\mathbf{v}_2,\mathbf{v}_3) = \arg(-\mathbf{v}_1\cdot\mathbf{v}_3 + (\mathbf{v}_1\cdot\mathbf{v}_2)(\mathbf{v}_2\cdot\mathbf{v}_3), \mathbf{v}_1\cdot(\mathbf{v}_2\times\mathbf{v}_3)) \quad (5)$$

for unit vectors $\mathbf{v}_1$, $\mathbf{v}_2$, and $\mathbf{v}_3$ (Quine, 1999). Here, arg(x, y) denotes the complex argument of (x, y), which is the angle between −180° and 180° formed by the x axis and the point (x, y) in the plane. The key for minimizing ambiguities is to compute the torsion angles by using only dot products of vectors, to avoid the need for changing frames between PAF_1 and PAF_2. The necessary dot products are

$$\begin{aligned}&\mathbf{u}_1\cdot\mathbf{u}_2 = \cos(59°) \\ &\mathbf{u}_1\cdot\mathbf{B}(\alpha_{PD1},\beta_{PD1}) = \cos(15°)\cos(\alpha_{PD1})\sin(\beta_{PD1}) \\ &\quad + \sin(15°)\cos(\beta_{PD1}) \\ &\mathbf{u}_2\cdot\mathbf{B}(\alpha_{PD1},\beta_{PD1}) = \cos(44°)\cos(\alpha_{PD1})\sin(\beta_{PD1}) \\ &\quad - \sin(44°)\cos(\beta_{PD1}) \\ &\mathbf{u}_2\cdot\mathbf{u}_3 = \cos(70°) \\ &\mathbf{u}_3\cdot\mathbf{u}_4 = \cos(65°) \\ &\mathbf{u}_3\cdot\mathbf{B}(\alpha_{PD2},\beta_{PD2}) = \cos(50°)\cos(\alpha_{PD2})\sin(\beta_{PD2}) \\ &\quad - \sin(50°)\cos(\beta_{PD2}) \\ &\mathbf{u}_4\cdot\mathbf{B}(\alpha_{PD2},\beta_{PD2}) = \cos(15°)\cos(\alpha_{PD2})\sin(\beta_{PD2}) \\ &\quad + \sin(15°)\cos(\beta_{PD2}) \end{aligned} \quad (6)$$

The scalar triple product in Eq. 5 does, however, give an ambiguity, known as a chirality ambiguity (Quine, 1999; Quine et al., 1997), when it is computed using dot products:

$$\mathbf{v}_1\cdot(\mathbf{v}_2\times\mathbf{v}_3) = \pm(1 - x^2 - y^2 - z^2 + 2xyz)^{1/2} \quad (7)$$

where

$$x = \mathbf{v}_1\cdot\mathbf{v}_2, \quad y = \mathbf{v}_2\cdot\mathbf{v}_3, \quad z = \mathbf{v}_1\cdot\mathbf{v}_3$$

Thus these equations yield 16 possible torsion angle pairs for every choice of (α_{PD1}, β_{PD1}) and (α_{PD2}, β_{PD2}). Here we will minimize this set based on the known α-helical secondary structure.

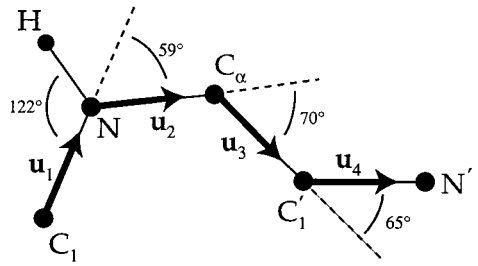

FIGURE 2 Bond direction unit vectors of a peptide plane and bond angles used for the calculations of backbone torsion angles.

RESULTS AND DISCUSSION

The chemical shift tensor element magnitudes have been determined by using single site labeled samples of M2-

TABLE 1 CSA values measured from single site ^{15}N-labeled M2-TMP powder samples (in ppm relative to saturated $^{15}NH_4NO_3$ solution)

Sites	σ_{11}	σ_{22}	σ_{33}	σ_{iso}
Val^{27}	31 ± 2	55 ± 2	199 ± 2	95 ± 2
Val^{28}	29	53	202	94.7
Ile^{32}	35	59	208	100.7
Ile^{33}	31	54	202	95.7
Ile^{35}	32	56	210	99.3
Ile^{39}	30	54	195	93
Ile^{42}	30	54	198	94

TMP. While the tensors were not determined in a hydrated lipid bilayer environment, they were determined as a powder prepared from a trifluoroethanol solution in which the samples are α-helical. Therefore, the tensors are characterized for the sites of interest in the conformation of interest (Table 1).

The PISEMA spectra of oriented M2-TMP samples with selective ^{15}N-labeling are displayed in Figs. 3, 5, and 6. The 2D contour plots display ^{15}N chemical shifts in the horizontal dimension and ^{15}N-^{1}H dipolar splittings in the vertical dimension, with the scale expanded by 1.22 to account for the experimental scaling of the dipolar dimension.

Fig. 3 shows the PISEMA spectrum of ^{15}N-Ile^{32,33,35,39,42}-labeled M2-TMP in hydrated DMPC lipid bilayers. For comparison, the conventional 1D chemical shift spectrum for this sample is shown at the top. While the peaks of four Ile sites between 118 and 129 ppm cannot be resolved in the 1D spectrum, they are resolved in this 2D spectrum and in the corresponding dipolar slices on the left side.

The spectral results are compared in Table 2 to the chemical shift data from single site labeled M2-TMP in similar bilayer preparations (spectra not shown). The assignments for Ile^{33}, Ile^{35}, and Ile^{42} and Val^{27} and Val^{28} are achieved from the single site labels. However, without the single site dipolar information, the assignments for Ile^{32} and Ile^{39} are tentative, based on a novel assignment strategy that recognizes a helical wheel pattern of resonances in the PISEMA spectra (Wang et al., 2000). Note that, while the chemical shift for Ile^{42} is within the error bar for Ile^{39} and Ile^{32}, the dipolar splitting from the single site label for Ile^{42} of 13.8 kHz confirms this assignment.

Normally, the sign of the dipolar splitting is considered to be ambiguous if $\Delta\nu$ is less than half-maximum (see Eq. 2). Fig. 4, however, shows that these peptide samples undergo an axial motion about the bilayer normal. Consequently, when this peptide sample is oriented with the bilayer normal perpendicular to the field, a single sharp line is observed rather than a powder pattern (a powder pattern would be seen if axial motion had not occurred). This means that the motionally averaged ^{15}N chemical shift and ^{15}N-^{1}H dipolar tensors are collinear. Because all of the σ_{obs} obtained are

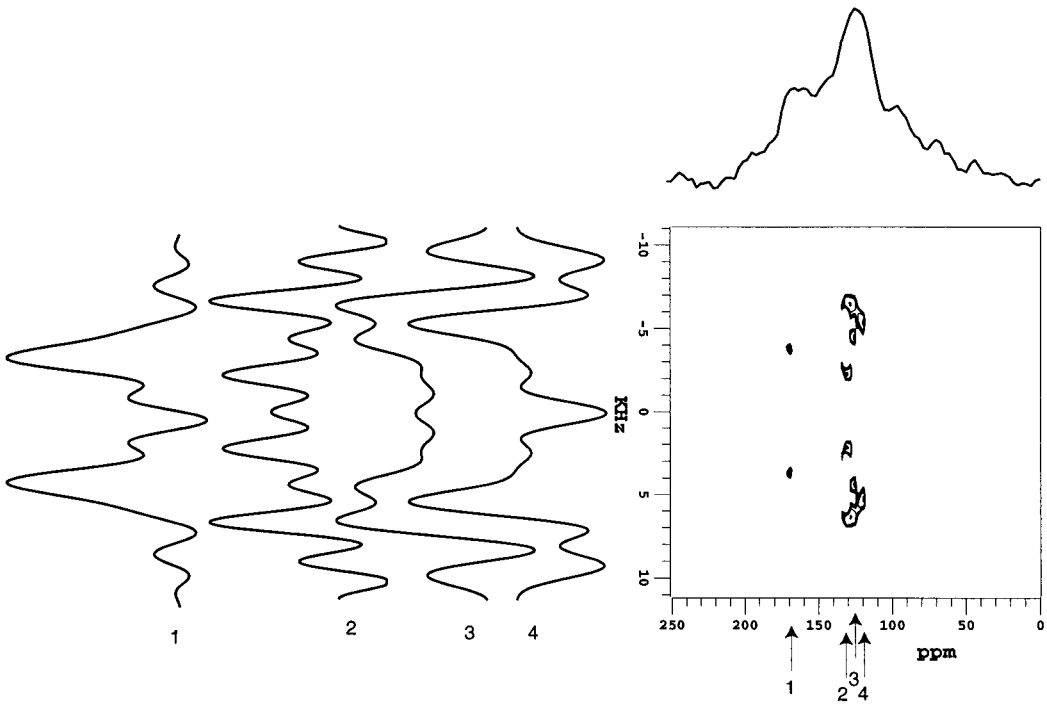

FIGURE 3 PISEMA spectrum of oriented ^{15}N-Ile^{32,33,35,39,42}-labeled M2-TMP in hydrated DMPC lipid bilayers. A conventional 1D spectrum is shown above. The slices on the left side represent the ^{15}N-^{1}H dipolar splittings corresponding to the chemical shifts indicated by the arrows in the contour plot. Chemical shifts are referenced to saturated $^{15}NH_4NO_3$ solution at 0 ppm.

TABLE 2 PISEMA results from multilabeled samples compared to single site labeled samples, and spectral interpretation of orientation

Sites	σ_{obs} (ppm) single site	σ_{obs} (ppm) PISEMA	$\Delta\nu$ (kHz) PISEMA	θ (°)*	α_{PD} (°)#	β_{PD} (°)#
Val[27]‡	136 ± 5	135 ± 3 (136)	13.7 ± 1.0 (14.0)	29.3 (28.8)	43.2 (42.8)	39.7 (39.3)
Val[28]‡	107	106 (106)	4.0 (4.0)	47.4 (47.4)	65.3 (65.3)	52.7 (52.7)
Ile[32]	124	129	4.4	46.7	82.2	46.6
Ile[33]	172	168	7.5	41.2	135.3	27.5
Ile[35]	116	118	10.6	35.5	38.5	47.6
Ile[39]	130	124	8.8	38.8	62.7	44.2
Ile[42]	129	127	13.2†	30.4	39.2	42.0

*With positive $\Delta\nu$, there are two possible solutions of (θ, $\pi - \theta$).
†Single site labeled sample resulted in a 13.8-kHz splitting.
‡The data in parentheses are from the sample with amantadine.
#There are four solutions of ($\pm\alpha_{PD}$, β_{PD}), ($\pi \pm \alpha_{PD}$, $\pi - \beta_{PD}$).

greater than their corresponding σ_{iso} values (Table 1), the $\Delta\nu$ values are all positive (Tian et al., 1998). This substantially reduces the potential structural ambiguities in the following analysis. Note that such a motion about an axis parallel to $\mathbf{B}_0$ for all of our samples, except Fig. 4 *B*, has no effect on the NMR observables.

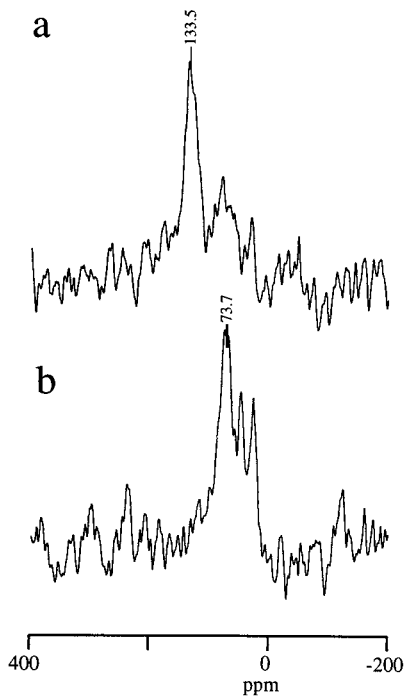

FIGURE 4 1D spectra of oriented ^{15}N-Leu^{43}-labeled M2-TMP in DMPC with the bilayer normal parallel (*a*) and perpendicular (*b*) to the magnetic field direction. The isotropic frequency is ~95 ppm. If global rotation about the bilayer normal had not occurred, a broad powder pattern would be observed for the perpendicular orientation. Furthermore, note that this global rotation has no impact on the observed orientational constraints obtained from samples aligned with the bilayer normal parallel to the magnetic field direction. The signal at 25 ppm is likely to be natural abundance ^{15}N from the choline headgroup. Because of the extensive dynamics of this choline site, the reproducibility of this intensity is poor, as it is very difficult to cross-polarize.

Based on these data, a variety of qualitative results can be identified. First, as previously noted (Kovacs and Cross, 1997; Kukol et al., 1999; Kovacs et al., 2000), the chemical shift and dipolar splitting values are not consistent with either a helix parallel to the bilayer normal or one perpendicular to it. Because the N-H axis and σ_{33} tensor elements are approximately parallel to the helix axis, helices that are parallel to the bilayer normal give rise to chemical shifts near σ_{33} and to $\Delta\nu$ values that are nearly maximal. In contrast, helices that are perpendicular give rise to chemical shifts near σ_{11}/σ_{22} and dipolar splittings that are at half-maximum and negative. The observed orientational constraints are variable and far from these extreme values; therefore, the helix has a considerable tilt.

Second, the substantial variation in dipolar splitting for nearly the same chemical shift (e.g., Ile[42] versus Ile[39]) illustrates the noncollinearity of the static ^{15}N chemical shift and ^{15}N-^{1}H dipolar tensors. The σ_{33} element is typically 17° from the N-H axis (Harbison et al., 1984; Oas et al., 1987; Mai et al., 1993). Third, the similarity of the orientational constraints for residues *i* and *i* + 7 (e.g., Ile[32] and Ile[39], Ile[35] and Ile[42]) suggests considerable uniformity for this α-helix. Even differences such as 8.8 kHz versus 4.4 kHz in dipolar splitting suggest a difference as small as 8° in the orientation of the N-H axis.

To investigate the structural influence of the channel inhibitor amantadine, the PISEMA spectra of oriented ^{15}N-Val[27,28]-labeled M2-TMP in hydrated DMPC bilayers with and without amantadine were acquired. For comparison, they are shown in Fig. 5 as overlaid spectra. The two splittings from Val[27] and Val[28] are well resolved in both chemical shift and dipolar dimensions. From conductivity measurements (Wang et al., 1993), the binding constant for amantadine has been established to be 3×10^6 M^{-1}. Therefore, the addition of an equal molar amount of M2-TMP and amantadine should result in a predominance of the complex. It has been suggested that amantadine binds in the vicinity of the Val[27,28] residues along the channel pore (Skehel, 1992; Hay, 1992; Wang et al., 1993). From our previous results and model (Kovacs and Cross, 1997), Val[27] should

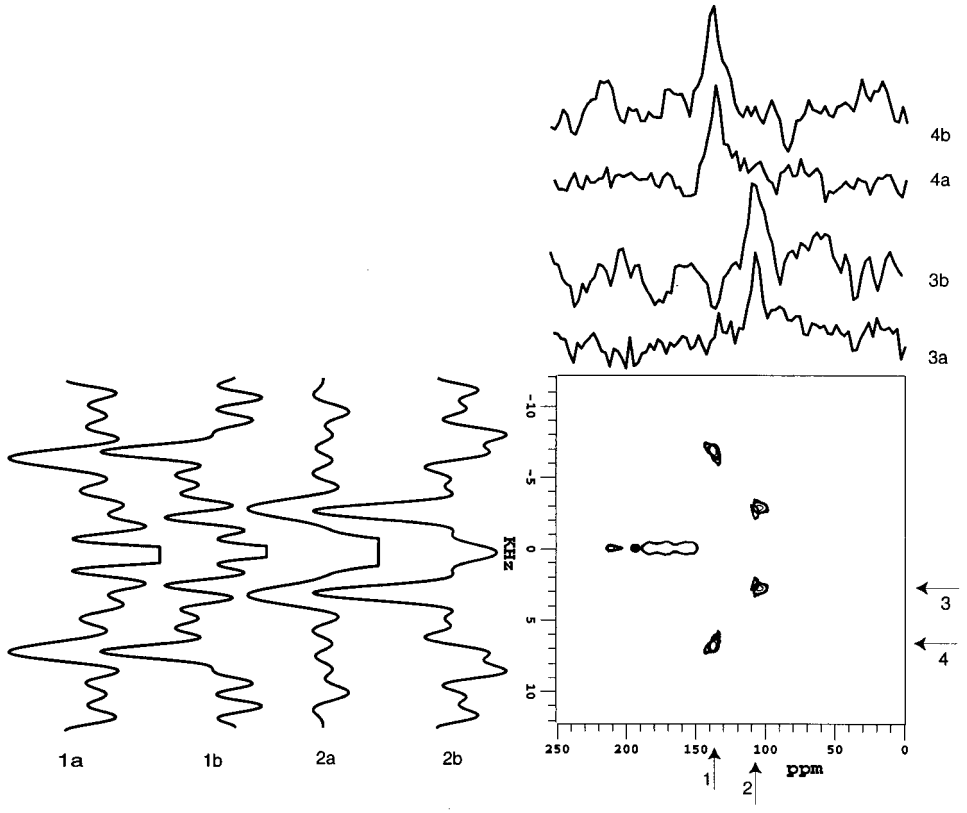

FIGURE 5 Overlay of PISEMA spectra of oriented ^{15}N-Val^{27,28}-labeled M2-TMP in hydrated DMPC lipid bilayers with (*b*) and without (*a*) amantadine bound. Dipolar and chemical shift slices are displayed for each resonance with and without amantadine bound. The negative contour artifacts near zero frequency in the dipolar dimension are deleted for clarity.

line the pore of the channel, while Val^{28} is oriented toward an adjacent helix. The observed differences in the dipolar splittings and in the chemical shifts are within their error bars for these two preparations, as clearly seen in the dipolar and chemical shift slices through the PISEMA spectra. Consequently, there is no evidence for a significant structural or orientational change for either site upon amantadine binding. Therefore, no evidence is presented here for amantadine interacting at these sites and directly blocking the channel pore. However, the lack of a change in the backbone structure and orientation does not refute this possibility, because amantadine is likely to be interacting directly with the side chains and not the backbone.

The improvement in spectral resolution shown in the chemical shift slices of the PISEMA spectra compared to the one-dimensional (1D) chemical shift spectra is nearly a factor of 2. Several different lipid environments and molar ratios have been tried to improve the 1D spectral resolution; however, little effect has been observed. PISEMA spectra of ^{15}N-Val^{27}-labeled M2-TMP in DOPC and DMPC bilayers are shown in Fig. 6. The slight difference in chemical shift and dipolar splitting possibly reflects a very small change in helix tilt due to the increased hydrophobic thickness of the DOPC bilayers. No difference, however, is seen in the linewidths, although they are substantially better than the 1D chemical shift spectra. Data from a T_2 measurement on this sample in DOPC yields a T_2 value of 750 μs, which suggests an intrinsic line width of 10 ppm (Fig. 7).

The line width in 1D spectra or in a projection of the PISEMA spectra in the chemical shift dimension displays a resonance width of ~20 ppm. In the 2D PISEMA spectra the heterogeneous broadening appears along a diagonal axis through 0 kHz at σ_{iso} = 96 ppm. Heterogeneous broadening in these 2D spectra will be constrained within the powder

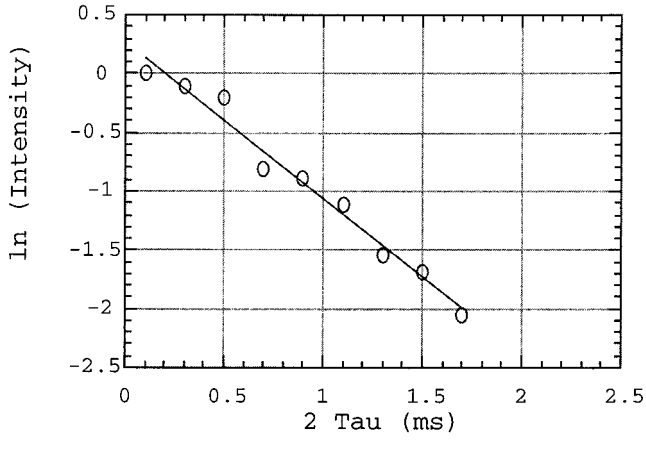

FIGURE 6 Overlay of PISEMA spectra of oriented ^{15}N-Val^{27}-labeled M2-TMP in hydrated DMPC and DOPC lipid bilayers. Dipolar and chemical shift slices are presented for the resonances in the two lipid environments (1,3 for DMPC; 2,4 for DMPC). The inserted peak corresponds to that for DMPC, plotted at a lower contour level and showing clearly the diagonally distributed resonance broadening.

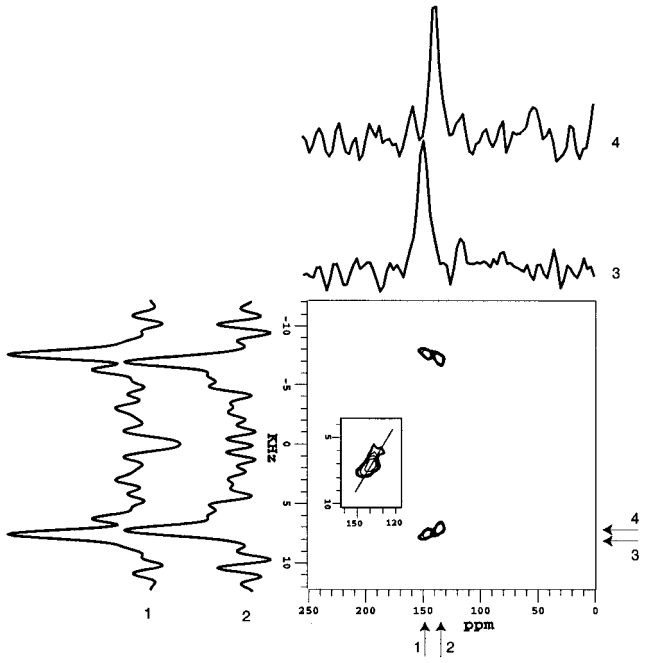

FIGURE 7 T_2 measurements of oriented ^{15}N-Val^{27}-labeled M2-TMP in DOPC bilayers at room temperature, obtained with cross-polarization and a variable delay Hahn echo.

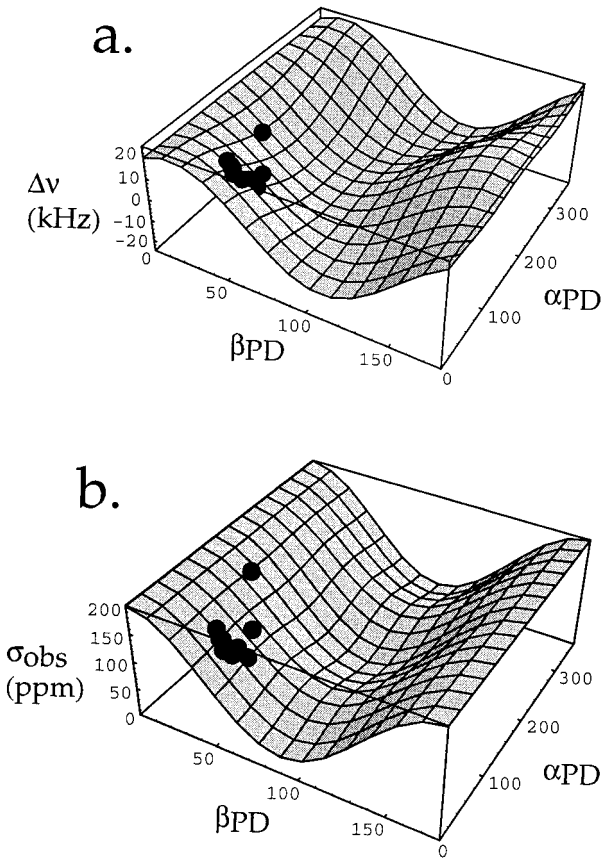

FIGURE 8 Orientation-dependent ^{15}N-^{1}H dipolar splitting (*a*) and chemical shift (*b*) as function of Euler angles α_{PD}, β_{PD} in M2-TMP. The CSA tensor values used in *b* are from the ^{15}N Val^{27}-labeled M2-TMP powder sample. The dots represent all possible solutions from Eqs. 1–3 before the elimination of ambiguities for the site in M2-TMP.

pattern of an unoriented sample, and because of the global motion this powder pattern lies on these diagonal axes. Thus the improved resolution in the chemical shift slices of the 2D PISEMA spectra (Fig. 6) results from a minimization of the heterogeneous broadening.

In Table 2, the θ angles derived from dipolar splittings are presented with the α_{PD} and β_{PD} angles determined with Eqs. 1–3. In Fig. 8, the dipolar splitting (*a*) and chemical shift (*b*) are plotted as a function of orientation angles α_{PD}, β_{PD} (ranging from 0 to 360° and 0 to 180° respectively), using the $\nu_{\|}$, α_{PNh}, β_{PNh} values mentioned above and typical σ_{11}, σ_{22}, σ_{33} values from the powder pattern of ^{15}N-Val^{27}-labeled M2-TMP. Both $\Delta\nu$ and σ_{obs} change more dramatically as a function of β_{PD} than as a function of α_{PD}. For σ_{obs}, this reflects the small asymmetry parameter of the amide ^{15}N CSA (typically $\eta \approx 0.2$). If η equaled 0, σ_{11} would equal σ_{22} and α_{PD} would have no effect on σ_{obs}. For $\Delta\nu$, it reflects the effect of both η and β_{PNh}. If β_{PNh} were also zero, then $\Delta\nu$ essentially would be independent of α_{PD}. Because β_{PNh} is significant (typically 17°), the influence of α_{PD} on $\Delta\nu$ generally is more pronounced. This partially explains why the five Ile sites, particularly Ile^{32}, Ile^{39}, and Ile^{42}, could not be resolved by their chemical shifts alone, but were resolvable by their dipolar splittings.

Because there is a limited data set from which it is not yet possible to calculate a unique molecular structure, we will take advantage of the knowledge that this polypeptide is predominantly α-helical (Duff et al., 1992; Kovacs and Cross, 1997), that the helices have an average tilt of 37° ± 3° (Kovacs et al., 2000), and that the α-helical geometry is well defined (Quine, 1999; Kovacs et al., 2000). The ambiguity in θ presented in Table 2 places the N–H orientation between 0° and 54.7° or 125.7° and 180°. For an α-helix the θ values must all be in one range or the other, because the N–H bond makes an angle in the range of ±17° with respect to the helix axis, which in turn makes an angle of 37° with the magnetic field axis. Moreover, this same argument eliminates all β_{PD} values greater than 90°. Therefore, only a single sign ambiguity remains in α_{PD} for each of the peptide planes, as shown in Table 3.

Many of the possible torsion angles calculated from Eqs. 4–7 can be eliminated based on steric hindrance information for Val and Ile residues in the α-helical region. Based on Ramachandran plots, β-branched amino acids have a more limited α-helical region than do other amino acids. In this analysis, the allowed α-helical region is taken from Creighten (1984). In Table 3, torsion angles within these dimensions are in boldface; borderline values within 10° of

TABLE 3 Orientations and corresponding torsion angles at Ile[32,33] and Val[27,28]

Sites	α_{PD1} (°)	β_{PD1} (°)	α_{PD2} (°)	β_{PD2} (°)	Φ (°)*	Ψ (°)*	τ (°)†
Val[27,28]	43	40	±65	53	*−52*	*−131*	*64*
	−43	40	±65	53	*−52*	*−131*	*19*
	43	40	±65	53	*−52*	*−35*	**35**
	−43	40	±65	53	*−52*	*−35*	**45**
	43	40	±65	53	*−105*	*−131*	*59*
	−43	40	±65	53	*−105*	*−131*	51
	43	40	±65	53	−105	−35	*15*
	−43	40	±65	53	−105	−35	*62*
	43	40	±115	127	**−83**	**−60**	*15*
	−43	40	±115	127	**−83**	**−60**	**41**
	43	40	±115	127	*−83*	*−156*	*76*
	−43	40	±115	127	*−83*	*−156*	51
	43	40	±115	127	*−136*	*−156*	*71*
	−43	40	±115	127	*−136*	*−156*	*66*
	43	40	±115	127	**−136**	**−60**	**29**
	−43	40	±115	127	**−136**	**−60**	*72*
Ile[32,33]	82	47	±135	28	*−23*	*−30*	49
	−82	47	±135	28	*−23*	*−30*	**47**
	82	47	±135	28	**−81**	**−30**	25
	−82	47	±135	28	**−81**	**−30**	*69*
	82	47	±135	28	*−23*	*−121*	*87*
	−82	47	±135	28	*−23*	*−121*	*7*
	82	47	±135	28	*−81*	*−121*	*79*
	−82	47	±135	28	*−81*	*−121*	55
	82	47	±45	153	*−128*	*−136*	*84*
	−82	47	±45	153	*−128*	*−136*	*85*

For angles Φ, Ψ, and τ, values in accepted ranges are in boldface, borderline values are in plain type, and outlying values are italicized.
*The allowed (Φ, Ψ) pairs for the α-helical region of a Ramachandran plot for β-branched amino acids are taken from Creighten (1984). Torsion angles within these dimensions are in boldface, borderline values within 10° of this region are in plain type, and outlying values are italicized.
†The τ values consistent with the global tilt of the helix are 37 ± 10° in boldface, borderline values are 37 ± 15° are in plain type, and outlying values are italicized.

this region are in plain type and outlying values are italicized. The most probable torsion angles, thus, are limited to (−83°, −60°) and (−136°, −60°) for Val[27] and (−81°, −30°) for Ile[32].

The transformation from one peptide plane to the next is defined by a (Φ, Ψ) torsion angle pair. From this transformation, the local helix axis direction vector for two adjacent peptide planes can be computed (Quine, 1999). Using α_{PD} and β_{PD} to define the magnetic field direction vector **B**, the tilt angle, τ, can be obtained from the dot product of the helix axis direction vector and **B**. Comparing computed tilts with the accepted tilt of 37° ± 3° provides another way to filter the possible orientations of **B**. In Table 3, tilts within the range of 37° ± 10° are in boldface; borderline values (37° ± 15°) are in plain type; and outlying values are italicized. Tilt calculations for Val[27] support the validity of the (Φ, Ψ) solutions and α_{PD}, β_{PD} solutions while solving the chirality ambiguity. For Ile[32], the unique torsion angle solution is supported and the chirality is solved.

Enhancement of spectral resolution has been achieved through 2D PISEMA of oriented M2-TMP samples. Information about ^{15}N chemical shift and ^{15}N-^{1}H dipolar interactions can be analyzed to derive specific site orientations leading to specific peptide plane orientations. In turn, these orientations lead to the structural solution for backbone peptide ϕ, ψ torsion angles in the transmembrane domain of M2 transmembrane peptide. From this solution set, helix axis orientations consistent with those previously described were found. Furthermore, the M2-TMP structure at residues Val[27,28] appears not to be distorted by amantadine binding.

The authors are indebted to the staff of National High Magnetic Field Laboratory NMR facility (A. Blue) and the staff of the Bioanalytical Synthesis and Service Laboratory (H. Hendricks and U. Goli) for their expertise and maintenance of the instruments essential for this effort.

This work has been supported by National Science Foundation (NSF) grant DMB 99-86036 to TAC and JRQ and by a NSF training grant supporting JKD (DBI 96-02233). This work was largely performed at the National High Magnetic Field Laboratory, supported by a NSF Cooperative Agreement (DMR-9527035) and the State of Florida.

REFERENCES

Bielecki, A., A. C. Kolbert, H. J. M. DE Groot, R. G. Griffin, and M. H. Levitt. 1990. Frequency-switched Lee-Goldburg sequences in solids. *Adv. Magn. Reson.* 14:111–124.

Creighton, T. E. 1984. Proteins: Structures and Molecular Principles. W. H. Freeman and Company, New York.

Cross, T. A., and S. J. Opella. 1994. Solid-state NMR structural studies of peptides and proteins in membranes. *Curr. Opin. Struct. Biol.* 4:574–581.

Cross, T. A., and S. J. Opella. 1983. Protein structure by solid state NMR. *J. Am. Chem. Soc.* 105:306–308.

Duff, K. C., and R. H. Ashley. 1992. The transmembrane domain of influenza A M2 protein forms amantadine-sensitive protein channels in planar lipid bilayers. *Virology.* 190:485–489.

Duff, K. C., S. M. Kelly, N. C. Price, and J. P. Bradshaw. 1992. The secondary structure of influenza A M2 transmembrane domain. A circular dichroism study. *FEBS Lett.* 311:256–258.

Feng, X., Y. K. Lee, D. Sandstrom, M. Eden, H. Maisel, A. Sebald, and M. H. Levitt. 1996. Direct determination of a molecular torsional angle by solid-state NMR. *Chem. Phys. Lett.* 257:314–320.

Fu, R., and T. A. Cross. 1999. Solid-state nuclear magnetic resonance investigation of protein and polypeptide structure. *Annu. Rev. Biophys. Biomol. Struct.* 28:235–268.

Gregory, D. M., M. A. Mehta, J. C. Shiels, and G. P. Drobny. 1997. Determination of local structure in solid nucleic acids using double quantum nuclear magnetic resonance spectroscopy. *J. Chem. Phys.* 107:28–42.

Gullion, T., and J. Schaeffer. 1989. Rotational-echo double-resonance NMR. *J. Magn. Reson.* 81:196–200.

Harbison, G. S., L. W. Jelinski, R. E. Stark, D. A. Torchia, J. Herzfeld, and R. G. Griffin. 1984. ^{15}N chemical shift and ^{15}N-^{13}C dipolar tensors for the peptide bond in [1-^{13}C]glycyl[^{15}N]glycine hydrochloride monohydrate. *J. Magn. Reson.* 60:79–82.

Hay, A. J. 1992. The action of adamantanamines against influenza A virus: inhibition of the M2 ion channel protein. *Semin. Virol.* 3:21–30.

Hester, R. K., J. L. Ackerman, B. L. Neff, and J. S. 1976. Waugh. Separated local field spectra in NMR: determination of structure of solids. *Phys. Rev. Lett.* 36:1081–1083.

Holsinger, L. J., and R. A. Lamb. 1991. Influenza virus M2 integral membrane protein is a homotetramer stabilized by formation of disulfide bonds. *Virology.* 183:32–43.

Hong, M., J. D. Gross, and R. G. Griffin. 1997. Site resolved determination of peptide torsion angle ϕ from the relative orientations of backbone N–H and C–H bonds by solid-state NMR. *J. Phys. Chem.* B101: 5869–5874.

Ketchem, R. R., W. Hu, and T. A. Cross. 1993. High-resolution conformation of gramicidin A in a lipid bilayer by solid state NMR. *Science.* 261:1457–1460.

Kovacs, F. A., and T. A. Cross. 1997. Transmembrane four-helix bundle of influenza A M2 protein channel: structural implications from helix tilt and orientation. *Biophys. J.* 73:2511–2517.

Kovacs, F. A., J. K. Denny, Z. Song, J. R. Quine, and T. A. Cross. 2000. Helix tilt of the M2 transmembrane peptide from influenza A virus: an intrinsic property. *J. Mol. Biol.* 295:117–125.

Kukol, A., P. D. Adams, L. M. Rice, A. T. Brunger, and I. T. Arkin. 1999. Experimentally based orientational refinement of membrane protein models: a structure for the influenza M2 H+ channel. *J. Mol. Biol.* 286:951–962.

Lamb, R. A., L. J. Holsinger, and L. H. Pinto. 1994. The influenza A virus M2 ion channel protein and its role in the influenza virus life cycle. *In* Receptor-Mediated Virus Entry into the Cell. E. Wimmer, editor. Cold Spring Harbor Laboratory, Cold Spring Harbor, New York. 303–321.

Lee, D. K., R. J. Wittebort, and A. Ramamoorthy. 1998. Characterization of ^{15}N chemical shift and ^{1}H-^{15}N dipolar coupling interactions in a peptide bond of uniaxially oriented and polycrystalline samples by one-dimensional dipolar chemical shift solid-state NMR spectroscopy. *J. Am. Chem. Soc.* 120:8868–8874.

Lee, M., and W. I. Goldburg. 1965. Nuclear-magnetic-resonance line narrowing by a rotating rf field. *Phys. Rev. A.* 140:1261–1271.

LoGrasso, P. V., L. K. Nicholson, and T. A. Cross. 1989. N–H bond length determinations and implications for the gramicidin channel conformation and dynamics from ^{15}N-^{1}H dipolar interaction. *J. Am. Chem. Soc.* 111:1910–1912.

Mai, W., W. Hu, C. Wang, and T. A. Cross. 1993. Orientational constraints as three-dimensional structural constraints from chemical shift anisotropy: the polypeptide backbone of gramicidin A in a lipid bilayer. *Protein Sci.* 2:532–542.

Marassi, F. M., A. Ramamoorthy, and S. J. Opella. 1997. Complete resolution of the solid-state NMR spectrum of a uniformly ^{15}N-labeled membrane protein in phospholipid bilayers. *Proc. Natl. Acad. Sci. USA.* 94:1739–1744.

Panayotov, P. P., and R. W. Schlesinger. 1992. Oligomeric organization and strain-specific proteolytic modification of the virion M2 protein of influenza A H1N1 viruses. *Virology.* 186:352–355.

Quine, J. R. 1999. Helix parameters and protein structures using quaternions. *Theochemistry.* 460:53–66.

Raleigh, D. P., M. H. Levitt, and R. G. Griffin. 1988. Rotational resonance in solid state NMR. *Chem. Phys. Lett.* 146:71–76.

Schmidt-Rohr, K. 1996. A double-quantum solid-state NMR technique for determining torsion angles in polymers. *Macromolecules.* 29: 3975–3981.

Skehel, J. J. 1992. Amantadine blocks the channel. *Nature.* 358:110–111.

Sugrue, R. J., and A. J. Hay. 1991. Structural characteristics of the M2 protein of influenza A viruses: evidence that it forms a tetrameric channel. *Virology.* 180:617–624.

Tang, P., C.-L. Juang, and G. S. Harbison. 1990. Intercalation complex of proflavine with DNA: structure and dynamics by solid-state NMR. *Science.* 249:70–72.

Tian, F., Z. Song, and T. A. Cross. 1998. Orientational constraints derived from hydrated powder samples by two-dimensional PISEMA. *J. Magn. Reson.* 135:227–231.

Tobler, K., M. L. Kelly, L. H. Pinto, and R. A. Lamb. 1999. Effect of cytoplasmic tail truncations on the activity of the M2 ion channel of influenza A virus. *J. Virol.* 73:9695–9701.

Wang, C., R. A. Lamb, and L. H. Pinto. 1994. Direct measurement of the influenza A virus M2 protein ion channel activity in mammalian cells. *Virology.* 205:133–140.

Wang, C., K. Takeuchi, L. H. Pinto, and R. A. Lamb. 1993. Ion channel activity of influenza A virus M2 protein: characterization of the amantadine block. *J. Virol.* 67:5585–5593.

Wang, J., Jeffrey K. Denny, C. Tian, S. Kim, Y. Mo, F. A. Kovacs, Z. Song, Z. Gan, R. Fu, J. R. Quine, and T. A. Cross. 2000. Imaging membrane protein helical wheels. *J. Magn. Reson.* 144:162–167.

Waugh, J. S. 1976. Uncoupling of local field spectra in nuclear magnetic resonance: determination of atomic positions in solids. *Proc. Natl. Acad. Sci. USA.* 73:1394–1397.

Weliky, D. P., and R. Tycko. 1996. Determination of peptide conformations by two-dimensional magic-angle-spinning NMR exchange spectroscopy with rotor synchronization. *J. Am. Chem. Soc.* 118:8487–8488.

Wu, C. H., A. Ramamoorthy, and S. J. Opella. 1994. High-resolution heteronuclear dipolar solid-state NMR spectroscopy. *J. Magn. Reson.* A109:270–272.